

Breaking Waves and Induced Currents on Coastal Structures

Entin A. Karjadi¹ and Nobuhisa Kobayashi²

Abstract: A horizontally two-dimensional, time dependent numerical model for obliquely incident shallow water waves with arbitrary incident angles is developed to predict the temporal and spatial variations of the free surface elevations and fluid velocities on inclined coastal structures. As a first attempt, use is made of periodic lateral boundary conditions, which limits the computations to regular waves on the slope of alongshore uniformity. The numerical method and the seaward and landward boundary algorithms are fairly general and expected to be applicable to irregular waves as well. The computed results for plunging waves on a rough 1:3.5 slope with the incident angles in the range of $0^\circ - 80^\circ$ are presented.

Introduction

The three-dimensional hydrodynamics processes on and around coastal structures are little known in comparison to the nearshore hydrodynamics on sandy beaches. As a result, no predictive model is available to predict breaking waves and induced currents on and around these inclined structures.

The available data are still limited because the experiments in directional wave basins to examine the effects of incident wave angles and directionality on design variables such as wave runup (De Wall and Van der Meer 1992) and wave reflection (Isaacson *et al.* 1996) were conducted mostly for straight structures on horizontal bottom. In addition, since these experiments include more design parameters and are much more time-consuming than unidirectional wave flume experiments, measurements are normally limited to free surface oscillations at several locations and do not provide detailed understanding of oblique wave dynamics on steep rough slopes.

Existing time-dependent models for waves on inclined coastal structures are limited mostly to normally-incident waves as reviewed by Kobayashi (1995). Liu *et al.* (1995) solved the finite-amplitude, shallow-water equations numerically to predict solitary wave runup around a circular island with a 1:4 side slope. Kobayashi and Karjadi (1996) and Kobayashi *et al.* (1997) developed numerical models for oblique irregular waves with small incident angles but these models can not be used to examine the

¹Department of Civil Engineering, Bandung Institute of Technology, Jalan Ganesha 10, Bandung 40132, Indonesia. E-mail: entin@coastal.udel.edu

²Professor and Associate Director, Center for Applied Coastal Research, University of Delaware, Newark, DE 19716, USA. E-mail: nk@coastal.udel.edu

effects of incident wave angles on the important quantities for the design of coastal structures.

In this paper, a two-dimensional, time-dependent numerical model for finite-amplitude, shallow-water waves with arbitrary incident angles is developed to examine the effects of incident wave angles on oscillatory and time-averaged wave characteristics on a steep rough slope. As a first attempt, use is made of periodic lateral boundary conditions. Consequently, computations are limited to regular waves on the slope of alongshore uniformity. Incident nonlinear waves at the toe of the slope are specified as input to the model. Reflected waves are predicted at the toe of the slope to examine the height, shape, angle and phase shift of reflected waves as a function of the incident wave angle. Computed waterline oscillations are analyzed to obtain wave runup, setup and run-down as a function of the incident wave angle. Furthermore, the computed spatial and temporal variations of the free surface elevation and horizontal velocities are analyzed to elucidate the detailed wave mechanics on the steep rough slope.

Numerical Model

The normalized depth-integrated continuity and horizontal momentum equations in shallow water may be expressed in the conservative vector form as

$$\frac{\partial \mathbf{U}}{\partial t} + \frac{\partial \mathbf{E}}{\partial x} + \frac{\partial \mathbf{F}}{\partial y} + \mathbf{G} = 0 \tag{1}$$

with

$$\mathbf{U} = \begin{bmatrix} h \\ hU \\ hV \end{bmatrix}; \quad \mathbf{E} = \begin{bmatrix} hU \\ hU^2 + h^2/2 \\ hUV \end{bmatrix}; \quad \mathbf{F} = \begin{bmatrix} hV \\ hUV \\ hV^2 + h^2/2 \end{bmatrix};$$

$$\mathbf{G} = \begin{bmatrix} 0 \\ h \frac{\partial z_b}{\partial x} + f(U^2 + V^2)^{1/2}U \\ h \frac{\partial z_b}{\partial y} + f(U^2 + V^2)^{1/2}V \end{bmatrix} \tag{2}$$

where the symbol are depicted in Fig. 1 with the prime indicates the physical variables; x' = horizontal coordinate taken to be positive landward with $x' = 0$ at the toe of the slope; y' = horizontal coordinate parallel to the toe alignment and taken to be positive in the downwave direction; h' = water depth; U' = depth- averaged cross-shore velocity; V' = depth-averaged alongshore velocity; g = gravitational acceleration; η' = free surface elevation above the still water level (SWL). The vertical coordinate z' is taken to be positive upward with $z' = 0$ at SWL. The bottom elevation is located at $z' = z'_b$ with $z'_b = (\eta' - h')$ and the spatial variation of z'_b is assumed to be known.

The normalized variables without the primes in (1) and (2) are defined as

$$t = \frac{t'}{T'}; \quad x = \frac{x'}{\sigma H'}; \quad y = \frac{y'}{\sigma H'}; \quad U = \frac{U'}{\sqrt{gH'}}; \quad V = \frac{V'}{\sqrt{gH'}} \tag{3}$$

$$h = \frac{h'}{H'}; \quad \eta = \frac{\eta'}{H'}; \quad z_b = \frac{z'_b}{H'}; \quad f = \frac{1}{2}\sigma f'_b; \quad \sigma = \frac{T'\sqrt{gH'}}{H'} \tag{4}$$

where T' and H' = incident wave period and height, respectively; f'_b = bottom friction factor which is allowed to vary spatially; and σ = ratio of the horizontal and vertical

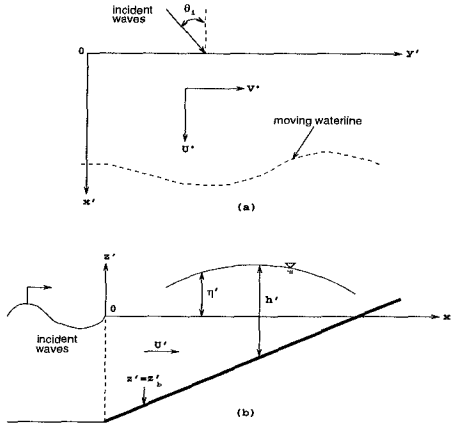


Figure 1: Definition sketch.

length scales which is assumed to satisfy $\sigma^2 \gg 1$ in shallow water (e.g., Kobayashi and Wurjanto 1992).

Equation (1) is solved numerically to compute the temporal and spatial variations of h , U and V where \mathbf{E} , \mathbf{F} and \mathbf{G} depend on \mathbf{U} only for given z_b and f . The mean water depth \bar{h} and the mean velocities \bar{U} and \bar{V} are then obtained by time-averaging the computed h , U and V where the overbar indicates time-averaging.

To interpret the computed spatial variations of \bar{h} , \bar{U} , and \bar{V} , the time-averaged continuity and momentum equations are derived from (1)

$$\frac{\partial}{\partial x}(\bar{h}\bar{U}) + \frac{\partial}{\partial y}(\bar{h}\bar{V}) = 0 \tag{5}$$

$$\frac{\partial}{\partial x}(S_{xx}) + \frac{\partial}{\partial y}(S_{xy}) + \bar{h} \frac{\partial \bar{\eta}}{\partial x} + \tau_{bx} = 0 \tag{6}$$

$$\frac{\partial}{\partial x}(S_{xy}) + \frac{\partial}{\partial y}(S_{yy}) + \bar{h} \frac{\partial \bar{\eta}}{\partial y} + \tau_{by} = 0 \tag{7}$$

with

$$S_{xx} = \overline{hU^2} + \frac{1}{2} \overline{(\eta - \bar{\eta})^2} ; \quad S_{xy} = \overline{hUV} ; \quad S_{yy} = \overline{hV^2} + \frac{1}{2} \overline{(\eta - \bar{\eta})^2} \tag{8}$$

$$\tau_{bx} = \overline{f(U^2 + V^2)^{1/2}U} ; \quad \tau_{by} = \overline{f(U^2 + V^2)^{1/2}V} \tag{9}$$

where S_{xx} , S_{xy} and S_{yy} = time-averaged momentum fluxes similar to radiation stresses (Longuet-Higgins 1970); and τ_{bx} and τ_{by} = time-averaged bottom shear stress in the x and y -directions. The accuracy of the time-dependent numerical model is checked using (5)-(7) with (8) and (9) because the computed h , U and V must satisfy the corresponding time-averaged equations.

The derivation of the depth-integrated energy equation corresponding to (1) is similar to that of Kobayashi and Wurjanto (1992). The time-averaging normalized

energy equation corresponding to (1) may be expressed as

$$\frac{\partial}{\partial x}(F_x) + \frac{\partial}{\partial y}(F_y) = -D_f - D_B \quad (10)$$

with

$$F_x = hU[\eta + \frac{1}{2}(U^2 + V^2)]; \quad F_y = hV[\eta + \frac{1}{2}(U^2 + V^2)]; \quad D_f = f(U^2 + V^2)^{1.5} \quad (11)$$

where F_x and F_y = time-averaged energy flux per unit width in the x and y -directions, respectively; and D_f and D_B = time-averaged rate of energy dissipation per unit horizontal area due to bottom friction and wave breaking, respectively. The dissipation rate D_B is related to the vertical variations of horizontal velocities and shear stresses outside the bottom boundary layer which are not predicted in this two-dimensional model. As a result, D_B is computed using (10) with (11) for the computed h , U and V using (1). The computed D_B must be positive or zero.

The computer program is developed using the MacCormack method (MacCormack 1969) which has been used successfully for the computation of two-dimensional transient open channel flow with bores (Chaudhry 1993). The finite difference grid of constant grid size Δx and Δy is used to solve (1). The values of Δx and Δy must be small enough to resolve the rapid spatial variation of the wave motion on the slope. The initial time $t = 0$ is taken to be the time when the incident wave train arrives at the seaward boundary and there is no wave action in the computation domain. The waterline in the numerical model is defined as the location where the instantaneous water depth h equals a small value δ , which is taken as $\delta = 10^{-3}$ in the subsequent computation. The time step size Δt varies for each time step and determined using an approximate numerical stability criterion proposed by Thompson (1990).

It is very difficult to specify incoming waves through the lateral boundaries into the computation domain and allow outgoing waves to propagate out of the computation domain without any numerical reflection from the lateral boundaries. As a first attempt, the periodic lateral boundary conditions are used here, although these conditions are appropriate only for regular waves on the slope of alongshore uniformity. For the periodic lateral boundaries, the nodes along the lateral boundaries are treated as the interior nodes.

The seaward boundary of the numerical model is located at the toe of the slope along the y -axis as shown in Fig. 1. In the region $x \leq 0$, the bottom is assumed to be horizontal so that a regular wave theory on the horizontal bottom may be used to specify the normalized incident wave train $\eta_i(t, y)$ at $x = 0$ in the following form:

$$\eta_i(t, y) = F_i(p) \quad \text{at} \quad x = 0 \quad (12)$$

with

$$p = t - \lambda y \quad ; \quad \lambda = \frac{T' \sqrt{gH'}}{L'} \sin \theta_i \quad (13)$$

where F_i = periodic function with respect to the phase p such that $F_i(p + 1) = F_i(p)$; L' = dimensional incident wavelength; θ_i = incident wave angle as shown in Fig. 1; and λ = inverse of the normalized alongshore wavelength. The alongshore wavelength, $L' / \sin \theta_i$, is constant on the slope of alongshore uniformity because of Snell's law (*e.g.*,

Dean and Dalrymple 1984). The function F_i depends on the wave theory used for a specific application. To satisfy the initial conditions of no wave action in the region $x \geq 0$, use is made of $\eta_i = tF_i$ for $0 \leq t < 1$ and $\eta_i = F_i$ for $t \geq 1$. To satisfy the periodic lateral boundary conditions, the computation domain width is taken as $0 \leq y \leq \lambda^{-1}$.

The seaward boundary algorithm for obliquely incident and reflected waves is not well established because no unique direction of propagation for characteristic variables exists for multidimensional hyperbolic equations including (1) (e.g., Thompson 1990). Several algorithms including that of Van Dongeren and Svendsen (1997) were tried to produce the periodic wave motion on the slope which satisfies the time-averaged equations (5)-(7). In addition, the computed reflected wave train must become periodic and propagate along the y -axis in a manner similar to (12). The algorithm satisfying these requirements is developed using the method of cross-shore characteristics.

A smoothing procedure is applied to damp numerical high-frequency oscillations which may appear at the rear of the steep front of a breaking wave. Use is made here of the relatively simple procedure described in Chaudhry (1993). The procedure of the numerical method and boundary conditions is described in detail in Kobayashi and Karjadi (1999).

Computed Wave Motions on Steep Slope

The developed two-dimensional model becomes practically the same as the one-dimensional model of Kobayashi *et al.* (1987) for normally-incident waves which was compared with the large-scale riprap tests reported by Ahrens (1975). Since there are no appropriate data available to verify this two-dimensional model, test 18 of Ahrens (1975) is used as an example in this paper. The computation results for test 12 with surging waves are presented in Kobayashi and Karjadi (1999).

For test 18, the riprap slope was 1:3.5; the still water depth at the toe of the slope, $d' = 4.57$ m; the incident wave period $T' = 4.2$ s; the incident wave height $H' = 1.01$ m; the median mass of the riprap, $M_{50} = 34$ kg; and the density of the riprap, $\rho_a = 2710$ kg/m³. The nominal diameter of the riprap defined as $D_{n50} = (M_{50}/\rho_a)^{1/3}$ was $D_{n50} = 0.232$ m. The test was limited to normally incident waves with $\theta_i = 0$. Computation is also made for the incident wave angle $\theta_i = 10^\circ, 20^\circ, 30^\circ, 40^\circ, 50^\circ, 60^\circ, 70^\circ$ and 80° . The ratio σ of the horizontal and vertical length scales defined in (4) is $\sigma = 13$, which satisfies the shallow water assumption of $\sigma^2 \gg 1$. The surf similarity parameter given by $\xi = \sigma \tan \theta / \sqrt{2\pi}$ is $\xi = 1.5$. The Ursell number $U_r = 5.7$ and the incident wave $\eta'_i(t', y')$ at the seaward boundary is computed using the Stokes second order theory (Kobayashi and Karjadi 1994). The bottom friction factor f'_b is taken as $f'_b = 0.3$ (Kobayashi *et al.* 1987). The damping coefficient κ for smoothing high-frequency numerical oscillations is taken to be very small ($\kappa = 0.01$) so as to minimize the numerical dissipation, although the numerical high-frequency oscillations become more visible as shown in Figs. 2 and 3 later.

The computation domain is taken as $0 \leq x \leq 1.95$ and $0 \leq y \leq \lambda^{-1}$ except for $\theta_i = 0$ because $\lambda = 0$ for $\theta_i = 0$. For $\theta_i = 0$, use is made of the value of λ corresponding to $\theta_i = 10^\circ$. The number of nodes in the x and y -directions are taken as 162 and 161,

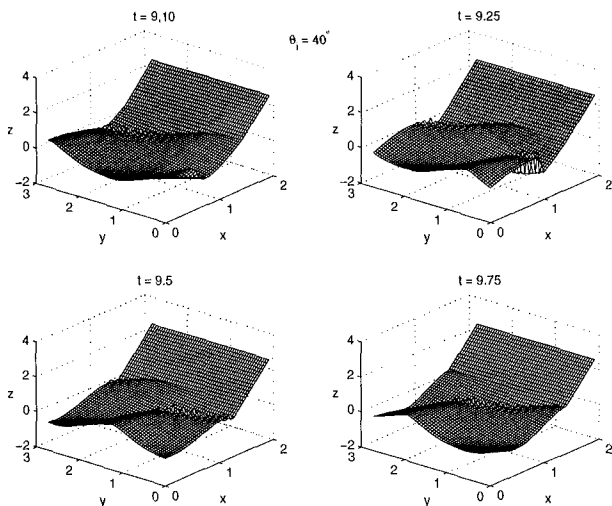


Figure 2: Spatial variations for free surface elevation η at time $t = 9, 9.25, 9.5, 9.75$ and 10.

respectively. The time step size Δt is on the order of 0.0003. The computation is made for $0 \leq t \leq 10$ and the time-averaging is performed for the last wave period $9 < t \leq 10$.

In the following, the computed results for $\theta_i = 40^\circ$ are presented as an example. Fig. 2 shows the spatial variations of the free surface elevation η at time $t = 9, 9.25, 9.5, 9.75$ and 10 for $\theta_i = 40^\circ$. The computed spatial variations at $t = 9$ and 10 are identical because the periodicity is established before $t = 9$. In the region of no water with $h = (\eta - z_b) = 0$, use is made of $\eta = z_b$ to depict the bottom elevation z_b of the slope. Fig. 2 indicates the oblique waves breaking and propagating along the slope.

Fig. 3 shows the temporal variations of η , U and V at $x = 0, 0.35, 0.71, 1.16$ and 1.40 along the cross-shore line at $y = 1.35$ where $\lambda^{-1} = 2.73$ for $\theta_i = 40^\circ$. The waterline at SWL is located at $x = 1.20$. The lower limit of the free surface elevation η at $x = 1.16$ and 1.40 corresponds to the bottom elevation z_b at those locations. The cross-shore velocity U at $x = 1.16$ and 1.40 indicates wave uprush ($U > 0$) of a short duration and wave down-rush ($U < 0$) of a longer duration. The longshore velocity V at $x = 1.16$ and 1.40 becomes more unidirectional ($V > 0$) because the large alongshore velocity occurs only during the short wave uprush. Fig. 3 also shows that the computed wave motion becomes periodic after a few waves unlike the longshore velocity V on a gentle smooth slope (Kobayashi and Karjadi 1994).

Fig. 4 shows the cross-shore variations of the maximum, mean and minimum values of η , U and V during the last wave period $9 < t \leq 10$. The root-mean-square (rms) values of the oscillatory components $(\eta - \bar{\eta})$, $(U - \bar{U})$ and $(V - \bar{V})$ are the standard deviations of η , U and V , which represent the oscillatory wave motion intensity.

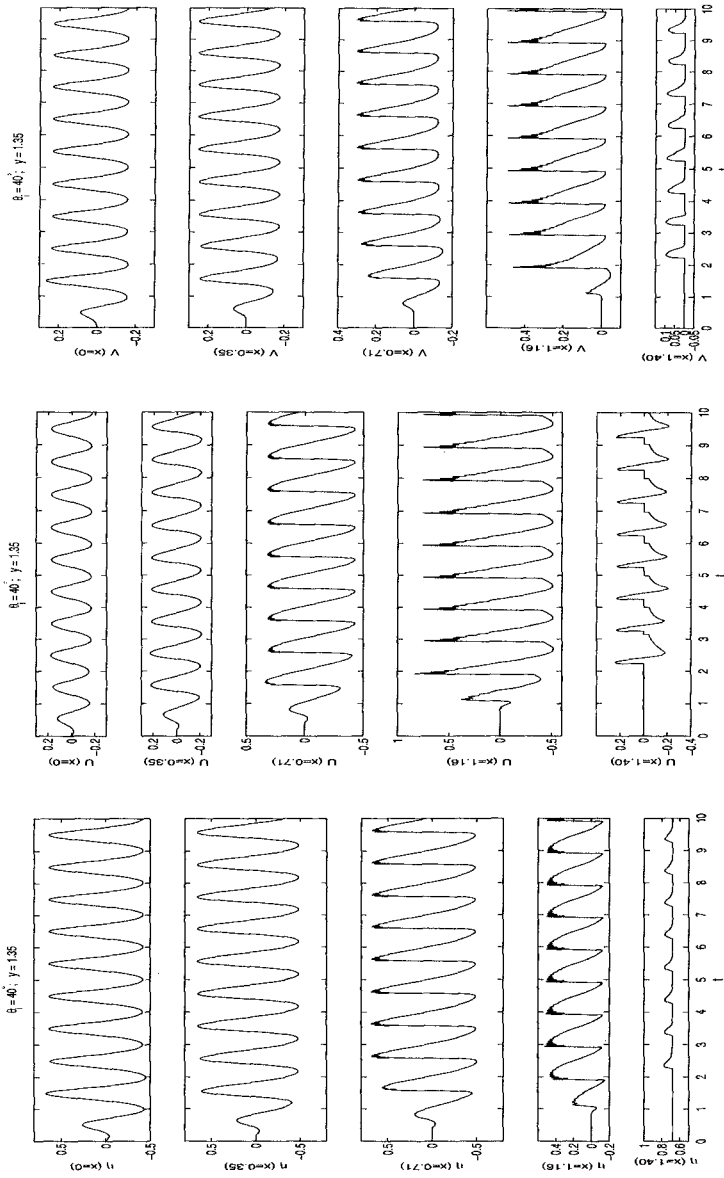


Figure 3: Temporal variations of free surface elevation η , cross-shore velocity U , and longshore velocity V at five cross-shore locations.

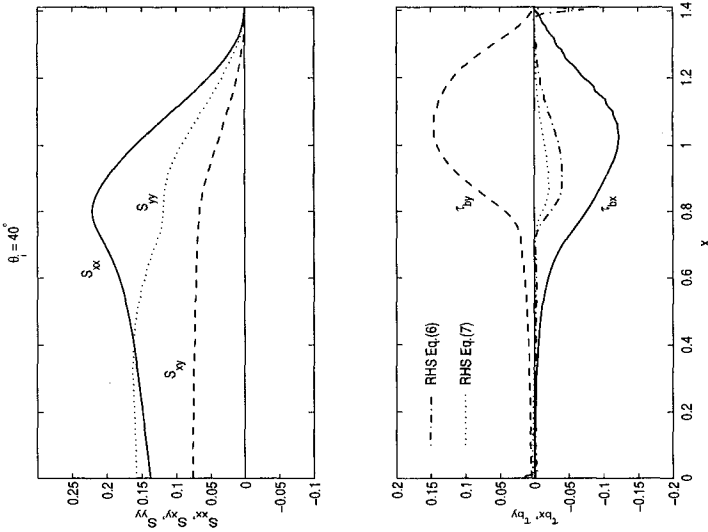


Figure 5: Cross-shore variations of time-averaged momentum quantities.

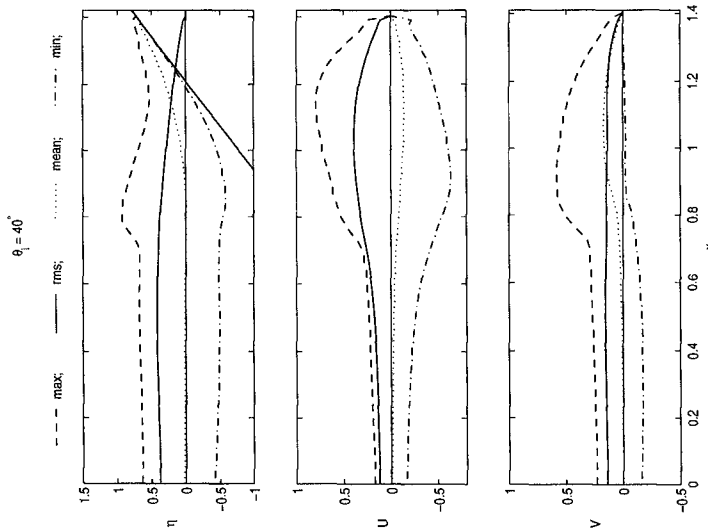


Figure 4: Cross-shore variations of maximum, root-mean-square, mean and minimum values of η , U and V .

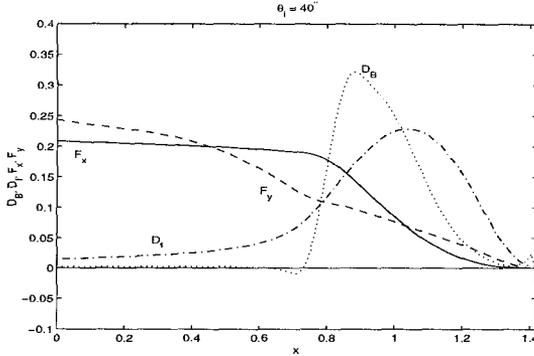


Figure 6: Cross-shore variations of time-averaged energy quantities.

The quantities shown in Fig. 4 are uniform alongshore. The 1:3.5 slope indicated by the solid straight line is added in the top panel to indicate the swash zone of wave uprush and down-rush on the slope. The rms wave intensity decreases landward in the swash zone. The largest U occurs near the still waterline while the largest η and V occur seaward of the still waterline. The mean cross-shore velocity \bar{U} is negative and represents the cross-shore return current. The mean alongshore velocity \bar{V} is the wave-induced longshore current which becomes as large as the standard deviation of V in the swash zone on the steep rough slope. The longshore current can become dominant on a gentle smooth slope (e.g., Kobayashi and Karjadi 1994).

The computed alongshore volume flux $\bar{h}\bar{V}$ is uniform alongshore. The time-averaged continuity equation (5) requires $\bar{h}\bar{U} = 0$ to satisfy the no flux condition into the impermeable slope. The computed cross-shore volume flux $\bar{h}\bar{U}$ satisfies this requirement.

The cross-shore variations of the momentum fluxes S_{xx} , S_{xy} and S_{yy} are depicted in Fig. 5, which also shows the bottom shear stresses τ_{bx} , τ_{by} and the time-averaged momentum equations (6) and (7). S_{xx} increases landward and decreases in the swash zone, whereas S_{yy} and S_{xy} is approximately constant seaward of the swash zone. The bottom shear stresses are important in the swash zone where the zone of $\tau_{bx} < 0$ and $\tau_{by} > 0$ corresponds approximately to the zone of $\bar{U} < 0$ and $\bar{V} > 0$ shown in Fig. 4. The computed time-averaged quantities are uniform alongshore. There is a small residual on the right hand side (RHS) of (6) and (7) due to the numerical dissipation, although the numerical damping coefficient $\kappa = 0.01$ is very small. For surging waves, the residuals for (6) and (7) were practically zero (Kobayashi and Karjadi 1999).

Fig. 6 shows the cross-shore variations of the time-averaged energy fluxes F_x and F_y and the time-averaged energy dissipation rates D_f and D_B due to bottom friction and wave breaking, respectively. The computed values of these quantities are uniform alongshore. Fig. 6 indicates that D_B is maximum at the location where η and V are maximum as shown in Fig. 4. The cross-shore and alongshore energy flux F_x and F_y decreases in the swash zone.

The reflected wave profile $\eta_r(t, y)$ along $x = 0$ is obtained as $\eta_r = (\eta - \eta_i)$ with η being the computed free surface elevation at $x = 0$. All the computed time series η_i and η_r at the 161 nodes along $x = 0$ for $0 \leq t \leq 10$ are plotted as a function of $p = (t - \lambda y)$ in Fig. 7. The 161 time series of η_i do not coincide for $-1 \leq p < 1$ because of the adjustment of η_i to satisfy the initial conditions of no wave action in the computation domain. The reflected wave profile η_r becomes periodic with respect to p after a few waves. This implies that the alongshore wavelengths of the incident and reflected waves are the same where λ for the incident waves is defined in (13). If the incident and reflected wavelengths are the same, $\sin \theta_i = \sin \theta_r$ where $\theta_r =$ reflected wave angle. This assumption is generally adopted to separate incident and reflected waves using linear wave theory (e.g., Isaacson *et al.* 1996).

The reflection coefficient r and the phase shift θ_r are estimated to examine their variations with respect to $\theta_i = 0^\circ - 80^\circ$. The estimation of r and θ_r is based on the periodic portions of η_i and η_r shown in Fig. 7. The reflection coefficient r is defined here as the ratio of the standard deviation of η_r to that of η_i . The phase shift ϕ_r is obtained as the shift of the crests of the incident and reflected wave profiles plotted as a function of $(t - \lambda y)$. For $\theta_i = 40^\circ$, the incident and reflected waves are in phase as shown in Fig. 7, where the phase shift remains the same by adding an integer to ϕ_r .

Fig. 8 shows the computed values of r and ϕ_r as a function of θ_i . The computed values of $r = 0.056$ for $\theta_i = 0^\circ$ is compared with available empirical formulas. The formula of Seelig and Ahrens (1995) predicts $r = 0.18$ for the rough impermeable slope assumed in the present computation. On the other hand, the formula of Davidson *et al.* (1996) predicts $r = 0.08$. The computed reflection coefficient r in Fig. 8 increases from $r = 0.056$ for $\theta_i = 0^\circ$ to $r = 0.32$ for $\theta_i = 80^\circ$. Most of the regular wave data by Isaacson *et al.* (1996) indicated the increase of r with $\theta_i = 0^\circ - 60^\circ$. As for the phase shift ϕ_r , Sutherland and O'Donoghue (1998) proposed two empirical formulas for the range $0^\circ \leq \theta_i \leq 60^\circ$. These formulas can be expressed as $\phi_r = 2.5(\cos \theta_i)^{0.71}$ and $\phi_r = 2.2(\cos \theta_i)^{0.625}$ for this specific case and are plotted in Fig. 8. The computed phase shifts are almost within the empirical curves for $0^\circ \leq \theta_i \leq 60^\circ$.

The waterline elevation Z_r' above SWL is defined as the free surface elevation measured by a hypothetical wire placed at a vertical distance of δ_r' above the bottom and parallel to the slope in the cross-shore direction. Since the nominal stone diameter was 23.2 cm, use is made of $\delta_r' = 0.4, 2$ and 4 cm which may represent the possible range of the roughness of the irregular bottom surface. All the computed time series of Z_r along the 161 cross-shore lines for $0 \leq t \leq 10$ are plotted as a function of $p = (t - \lambda y)$ for $\delta_r' = 0.4, 2$ and 4 cm. Fig. 9 shows that the computed waterline oscillations become periodic after a few waves. The normalized alongshore wavelength of the waterline oscillations on the slope is the same as the incident alongshore wavelength λ^{-1} at $x = 0$. This indicates the validity of Snell's law for obliquely incident waves on the slope of alongshore uniformity. Fig. 9 also indicates that wave down-rush with a thin layer of water is sensitive to the wire height δ_r' .

The periodic portions of Z_r are used to obtain the maximum, mean, minimum and standard deviation and values of Z_r . The maximum Z_r is the wave runup R_u , which is shown in Fig. 10, and the minimum Z_r is the wave rundown. The wave runup R_u is not sensitive to $\delta_r' = 0.4 - 4$ cm. The computed value of R_u for $\theta_i = 0^\circ$ is 1.05 in comparison

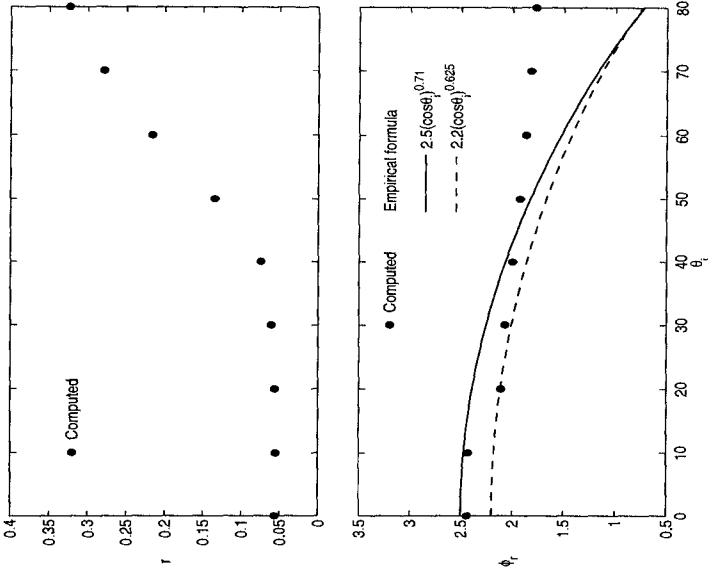


Figure 8: Reflection coefficient r and phase shift ϕ_r as a function of incident wave angles θ_i , in degrees.

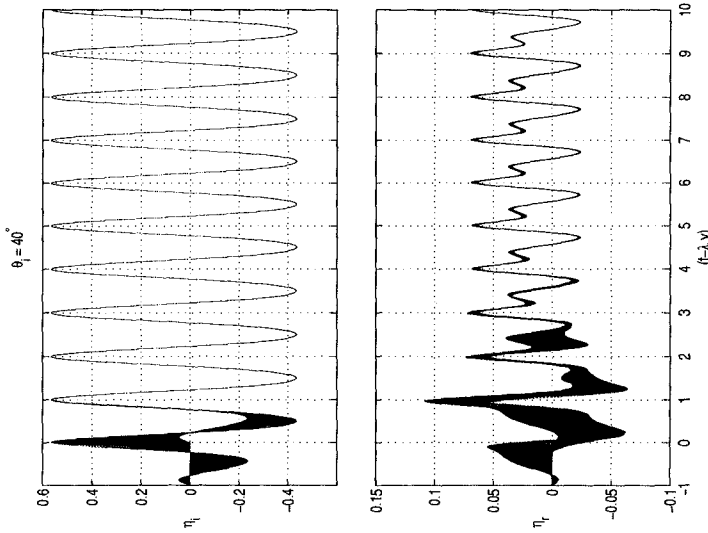


Figure 7: Incident and reflected wave profiles as a function of shifted time $(t - \lambda y)$.

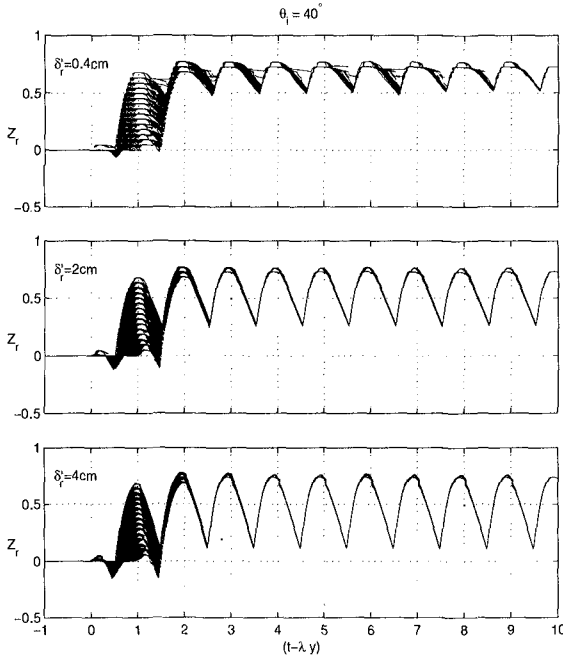


Figure 9: Waterline elevations Z_r for water depth $\delta_r' = 0.4, 2$ and 4 cm as a function of shifted time $(t - \lambda y)$.

to $R_u = 1.06$ observed visually in test 18 by Ahrens (1975). The empirical relationship shown in Fig. 10 is based on the runup reduction factor $\gamma = R_u(\theta_i)/R_u(\theta_i = 0^\circ)$ proposed by De Wall and Van der Meer (1992). For unidirectional irregular waves, $\gamma = 1$ for $0^\circ \leq \theta_i \leq 10^\circ$, $\gamma = \cos(\theta_i - 10^\circ)$ for $10^\circ \leq \theta_i \leq 63^\circ$, and $\gamma = 0.6$ for $63^\circ \leq \theta_i \leq 80^\circ$. The decrease of the computed regular wave runup with the increase of θ_i is consistent for small θ_i but larger for large θ_i . On the other hand, Fig. 11 shows the wave runup R_u , the mean waterline elevation \bar{Z}_r , the standard deviation σ_r , and the wave run-down R_d for $\delta_r' = 2$ cm. The computed R_u , \bar{Z}_r and R_d decrease with the increase of θ_i , whereas the standard deviation of Z_r representing the intensity of the waterline oscillation about the mean \bar{Z}_r remains approximately constant. Correspondingly, the value of $(R_u - R_d)$ remains approximately constant.

Conclusions

A two-dimensional, time-dependent numerical model for finite-amplitude, shallow-water waves with arbitrary incident angles is developed to provide an additional tool for the design of coastal structures. The utility of this numerical model is to obtain the detailed wave motions in the vicinity of the still waterline which are difficult to

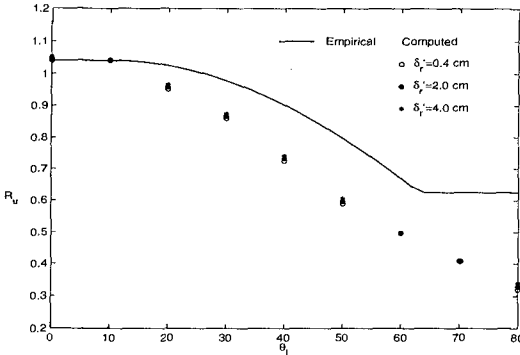


Figure 10: Wave runup R_u for $\delta_r = 0.4, 2$ and 4 cm as a function of θ_i in degrees.

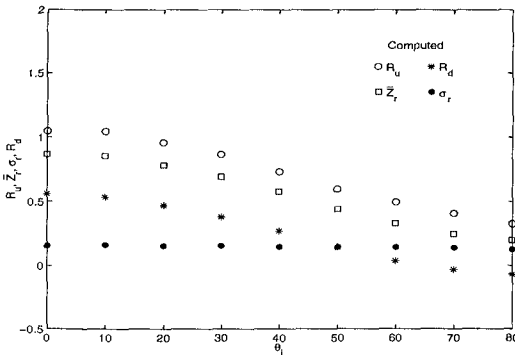


Figure 11: Wave runup R_u , setup \bar{Z}_r , standard deviation σ_r , and run-down R_d for $\delta_r = 2$ cm as a function of θ_i in degrees.

measure in experiments. The use of periodic lateral boundary conditions has limited the present computations to regular waves on the slope of alongshore uniformity. The numerical method and the seaward and landward boundary algorithms presented here are general and expected to be applicable to irregular waves as well.

The time-averaged continuity, momentum and energy equations are used to check the accuracy of the numerical model as well as to examine the spatial variations of the time-averaged quantities. For the computed plunging waves, the energy dissipation rate due to wave breaking is significant as shown in Fig. 6. This dissipation appears to have produced the residuals in (6) and (7) as shown in Fig. 5. The computed reflected waves and waterline oscillations are shown to have the same alongshore wavelength as the incident waves.

The numerical model will need to be compared with new experiments that will

include the temporal and spatial variations of the free surface elevation and velocities. It is also essential to generalize the lateral boundary algorithm for irregular waves. An algorithm similar to the seaward boundary algorithm used here might be applied if the incident waves at the lateral boundaries could be specified as input.

Acknowledgement

This work was supported by the National Oceanic and Atmospheric Administration Office of Sea Grant, Department of Commerce, under Grant No. NA56RG0147 (Project SG97 R/OE-23).

References

- Ahrens, J.P. (1975). "Large wave tank tests of riprap stability." Tech. Memo No. 51, U.S. Army Coast. Engrg. Res. Ctr., Ft. Belvoir, Va.
- Chaudhry, M.N. (1993). *Open-channel flow*. Prentice Hall, Englewood Cliffs, N.J.
- Davidson, M.A., Bird, P.A.D., Huntley, D.A., and Bullock, C.N. (1996). "Prediction of wave reflection from rock structures: An integration of field & laboratory data." *Proc., 25th Coast. Engrg. Conf.*, ASCE, New York, N.Y., 2, 2077-2086.
- Dean, R.C., and Dalrymple, R.A. (1984). *Water wave mechanics for engineers and scientists*. Prentice Hall, Englewood Cliffs, N.J.
- De Wall, J.P., and Van der Meer, J.W. (1992). "Wave runup and overtopping on coastal structures." *Proc., 23rd Coast. Engrg. Conf.*, ASCE, New York, N.Y., 2, 1758-1771.
- Isaacson, M., Papps, D., and Mansard, E. (1996). "Oblique reflection characteristics of rubble-mound structures." *J. Wtrwy., Port, Coast., and Oc. Engrg.*, ASCE, 122(1), 1-7.
- Kobayashi, N. (1995). "Numerical models for design of inclined coastal structures." *Wave forces on inclined and vertical wall structures*, N. Kobayashi and Z. Demirebilek, eds., ASCE, New York, N.Y., 118-138.
- Kobayashi, N., and Karjadi, E.A. (1994). "Swash dynamics under obliquely incident waves." *Proc., 24th Coast. Engrg. Conf.*, ASCE, New York, N.Y., 2, 2155-2168.
- Kobayashi, N., and Karjadi, E.A. (1996). "Obliquely incident irregular waves in surf and swash zones." *J. Geophys. Res.*, 101(C3), 6527-6542.
- Kobayashi, N., Karjadi, E.A. (1999). "Obliquely incident wave reflection and runup on steep rough slope." *J. Wtrwy., Port, Coast., and Oc. Engrg.*, ASCE, (submitted).
- Kobayashi, N., Karjadi, E.A., and Johnson, B.D. (1997). "Dispersion effects on longshore currents in surf zones." *J. Wtrwy., Port, Coast., and Oc. Engrg.*, ASCE, 123(5), 240-248.
- Kobayashi, N., Otta, A.K., and Roy, I. (1987). "Wave reflection and runup on rough slopes." *J. Wtrwy., Port, Coast., and Oc. Engrg.*, ASCE, 113(3), 282-298.
- Kobayashi, N., and Wurjanto, A. (1992). "Irregular wave setup and run-up on beaches." *J. Wtrwy., Port, Coast., and Oc. Engrg.*, ASCE, 118(4), 368-386.
- Liu, P.L.-F., Cho, Y.S., Briggs, M.J., Kanoglu, U., and Synolakis, C.E. (1995). "Runup of solitary waves on a circular island." *J. Fluid Mech.*, 302, 259-285.
- Longuet-Higgins, M.S. (1970). "Longshore currents generated by obliquely incident sea waves." *J. Geophys. Res.*, 75(33), 6778-6801.
- MacCormack, R.W. (1969). "The effects of viscosity in hypervelocity impact cratering." Pap. 69-354, *Am. Inst. Aeronaut. and Astronaut.*, New York, N.Y.
- Seelig, W.N., and Ahrens, J.P. (1995). "Wave reflection and energy dissipation by coastal structures." *Wave forces on inclined and vertical wall structures*, N. Kobayashi and Z. Demirebilek, eds., ASCE, New York, N.Y., 28-51.
- Sutherland, J., and O'Donoghue, T. (1998). "Wave phase shift at coastal structures." *J. Wtrwy., Port, Coast. and Oc. Engrg.*, ASCE, 124(2), 90-98.
- Thompson, K.W. (1990). "Time-dependent boundary conditions for hyperbolic systems, II." *J. Comp. Phys.*, 89, 439-461.
- Van Dongeren, A.R., and Svendsen, I.A. (1997). "Absorbing-generating boundary condition for shallow water models." *J. Wtrwy., Port, Coast., and Oc. Engrg.*, ASCE, 123(6), 303-313.